Supporting Information

Saranathan et al. 10.1073/pnas.0909616107

SI Text

We use the following formula to convert between chitin filling fraction, f_c, and average refractive index, n_{avg}:

$$n_{avg} = \sqrt{f_c n_c^2 + (1 - f_c) n_{air}^2}, \quad \textbf{[S1]}$$

where n_c is the refractive index of chitin (1) (1.56), and n_{air} is that of air.

SI Materials and Methods. ***Specimens.*** We analyzed the nanostructure and structural color production in five butterfly species from two different lepidopteran families (Table S1): The green dorsal wing scales of the papilionids, *Parides sesostris* and *Teinopalpus imperialis*; and the green ventral wing scales of the lycaenids, *Callophrys dumetorum*, *Callophrys* (formerly *Mitoura*) *gryneus*, and *Cyanophrys herodotus* (a close congener of *Cyanophrys remus*). Small (<1 cm^2) samples of structurally colored butterfly wings were taken from specimens obtained from the Snow Entomology Collection of the University of Kansas Museum of Natural History and Yale Peabody Museum of Natural History.

Indexing small angle X-ray scattering (SAXS) data. We consulted the International Union of Crystallography (IUCr) International Tables for Crystallography (2) to index the SAXS peaks and assign crystallographic space group symmetries to the butterfly nanostructures.

Optical microscopy. Light micrographs of the specimens were obtained on a Zeiss AxioCam stereo light microscope using a 0.63× objective at various magnifications.

Electron microscopy. We followed standard embedding procedures for TEM (3). For SEM, freeze-fractured samples were gold coated and studied on an ISI-SS40 SEM and a Philips XL 30 environmental SEM, at a range of tilt angles from −10° to 45°.

Fibre optic spectrophotometry. Normal-incidence reflectance spectra of the structurally colored butterfly wings were measured with an Ocean Optics S2000 fiber optic spectrophotometer and an Ocean Optics deuterium-halogen light source on a Macintosh computer, using standard procedure (3). The S2000 provides 2,048 data points between 178 and 879 nm. Reflectance was measured using normal incident light at a distance of 6 mm from a 3 mm^2 patch of the integument with a 500 ms integration time and calibrated using an Ocean Optics Spectralon matte white standard.

Level set triply periodic minimal surface (TPMS) modeling. The center of the invaginating lipid-bilayer plasma membrane during the development of the butterfly scale nanostructures is an example of a TPMS that divides a volume into two bicontinuous, nonintersecting networks, namely Schoen's *G* (space group *Ia3d*) surface (4). The interface of the two phases can also be described as constant mean curvature (CMC) surfaces because they possess net zero curvature throughout their volume, or as constant thickness (CT) surfaces. These CMC and CT surfaces can be conveniently modeled in silico by their level set approximations (Eq. **2** from the main text) (5, 6).

Three-dimensional level set approximations (6) of gyroid structures were volume rendered using MATLAB. Artificial sections of appropriate thicknesses, simulating SEM and TEM sections, were made from the 3D volumes visualized using the University of California, San Francisco Chimera package (http://www.cgl.ucsf.edu/chimera). The volume fractions of chitin, obtained from published sources (3, 5) and our own TEM images, as well as from SAXS data (Tables S1 and S2) were used to make the simulated sections biologically relevant.

1. Vukusic P, Sambles JR, Lawrence CR, Wootton RJ (1999) Quantified interference and diffraction in single Morpho butterfly scales. *P Roy Soc Lond B Bio* 266(1427): 1403–1411.
2. Hahn T (2006) The 230 space groups. *IUCr International Tables for Crystallography* Space-group symmetry, (Springer, New York), Vol A, Ch 7.1, pp 112–717.
3. Prum RO, Quinn T, Torres RH (2006) Anatomically diverse butterfly scales all produce structural colours by coherent scattering. *J Exp Biol* 209:748–765.
4. Schoen AH (1970) Infinite periodic minimal surfaces without self-intersections. (NASA Research Center, Cambridge, MA), NASA Technical Note C-98.
5. Michielsen K, Stavenga DG (2008) Gyroid cuticular structures in butterfly wing scales: Biological photonic crystals. *J R Soc Interface* 5(18):85–94.
6. Wohlgemuth M, Yufa N, Hoffman J, Thomas EL (2001) Triply periodic bicontinuous cubic microdomain morphologies by symmetries. *Macromolecules* 34(17):6083–6089.
7. Kertész K, et al. (2006) Gleaming and dull surface textures from photonic-crystal-type nanostructures in the butterfly *Cyanophrys remus*. *Phys Rev E* 74(2, Pt 1):021922, http://pre.aps.org/abstract/PRE/v74/i2/e021922.
8. Almsherqi ZA, Kohlwein SD, Deng Y (2006) Cubic membranes: A legend beyond the Flatland* of cell membrane organization. *J Cell Biol* 173(6):839–844.
9. Hajduk DA, et al. (1995) A reevaluation of bicontinuous cubic phases in starblock copolymers. *Macromolecules* 28:2570–2573.
10. Hajduk DA, et al. (1994) The gyroid: A new equilibrium morphology in weakly segregated diblock copolymers. *Macromolecules* 27:4063–4075.
11. Argyros A, Large MCJ, McKenzie DR, Cox GC, Dwarte DM (2002) Electron tomography and computer visualization of a three-dimensional 'photonic' crystal in a butterfly wing-scale. *Micron* 33:483–487.

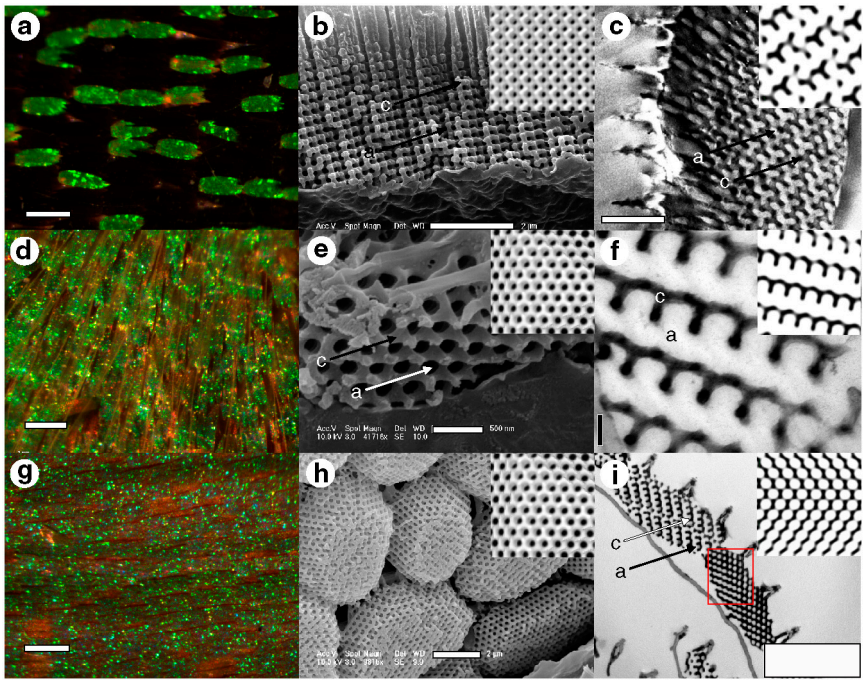

Fig. S1. Anatomy of the structural color producing nanostructure in papilionid and lycaenid butterflies. (*A*) Light micrograph of the dorsal wing cover scales of *Teinopalpus imperialis* (Papilionidae). (Scale bar: 150 μm.) (*B*) SEM image of the lateral surface of the wing scale nanostructure of *T. imperialis* showing fused polycrystalline domains beneath columnar windows created by a network of ridges and spaced cross-ribs. The fractured face features a square lattice of air holes in chitin. (Scale bar: 2 μm.) (*Inset*) Simulated SEM (100) projection from a thick slab of a level set single gyroid nanostructure. (*C*) TEM image of the *T. imperialis* nanostructure showing a distinctive trifoliate motif, uniquely characteristic of the (332) plane of the gyroid morphology. (Scale bar: 1 μm.) (*Inset*) A matching simulated (332) TEM section of a level set single gyroid model. (*D*) Light micrograph of the ventral wing cover scales of *Callophrys dumetorum* (Lycaenidae). The opalescent highlights are produced by randomly oriented crystallite domains. (Scale bar: 100 μm.) (*E*) SEM image of the lateral surface of the wing scale nanostructure of *C. dumetorum*. The fractured face features a triangular lattice of air holes in chitin. (Scale bar: 500 nm.) (*Inset*) Simulated SEM (111) projection of a thick slab of a level set single gyroid nanostructure. (*F*) TEM image of the *C. dumetorum* nanostructure showing a distinctive motif, uniquely characteristic of the (211) plane of the gyroid morphology. (Scale bar: 200 nm.) (*Inset*) A matching simulated (211) TEM section of a level set single gyroid model. (*G*) Light micrograph of the ventral wing cover scales of *Cyanophrys herodotus* (Lycaenidae). The opalescent highlights are produced by randomly oriented crystallite domains. (Scale bar: 100 μm.) (*H*) SEM image of the ventral surface of a *C. herodotus* scale showing disjoint crystallites. (Scale bar: 2 μm.) (*Inset*) Simulated SEM (111) section from a thick slab of a level set single gyroid nanostructure. (*I*) TEM image of the *C. herodotus* ventral wing scale nanostructure (from ref. 7) showing distinctive motifs, uniquely characteristic of the (211) and (110) planes of the gyroid morphology. (Scale bar: 2 μm.) (*Inset*) A matching simulated (110) TEM section of a level set single gyroid model corresponding to the motif within the red box. c, chitin; a, air void. (Reprinted figure with permission from ref. 7. Copyright 2006 by the American Physical Society).

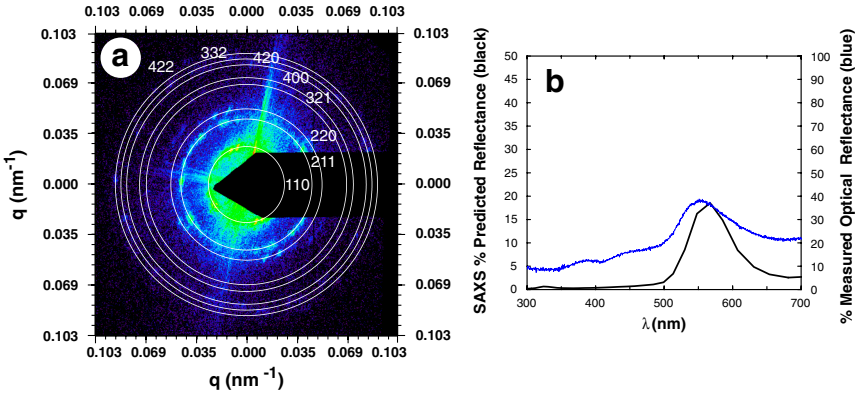

Fig. S2. (*A*) Representative 2D SAXS pattern (original image 1340 × 1300 pixels), and (*B*) a comparison of predicted reflectance (black line) from an azimuthal average of the SAXS pattern against measured optical reflectance (blue line), for *Callophrys dumetorum*. The false color scale in *A* corresponds to the logarithm of the X-ray scattering intensity. The radii of the concentric circles are given by the peak scattering wave vector (q_{max}) times the moduli of the assigned *hkl* indices, where *h*, *k*, and l are integers allowed by the single gyroid ($I4_132$) symmetry space group (IUCr International Tables for Crystallography, ref. 2). See main text for other details.

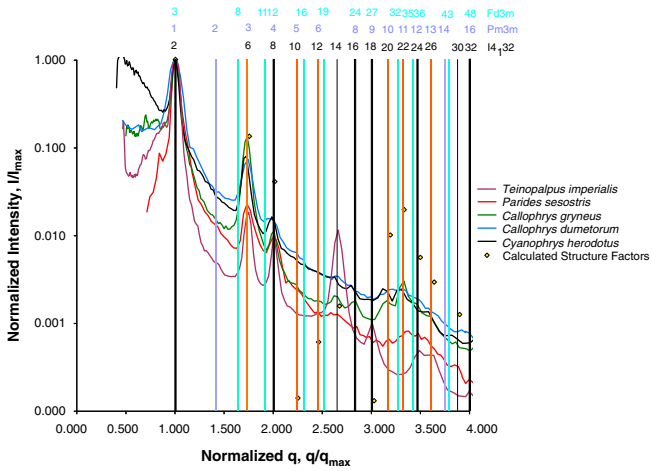

Fig. S3. Normalized azimuthally averaged X-ray scattering profiles (intensity I/I_{max} vs. scattering wave vector q/q_{max}) calculated from the respective 2D SAXS patterns for *Teinopalpus imperialis, Parides sesostris, Callophrys (Mitoura) gryneus, Callophrys dumetorum*, and *Cyanophrys herodotus*. The sets of color-coded vertical lines correspond to the expected Bragg peak positional ratios for the single gyroid ($I4_132$; black), single diamond (*Fd3m*; cyan), and simple primitive (*Pm3m*; mauve) cubic crystallographic space groups, presented together for direct comparison and positive exclusion of all but one of these plausible alternative cubic symmetries. Allowed reflections common to all three cubic space groups are highlighted by thick black lines, whereas those shared between $I4_132$ and *Pm3m* are shown in orange. The numbers above the vertical lines are squares of the moduli of the Miller indices (*hkl*) for the allowed reflections, from each of the three space groups.

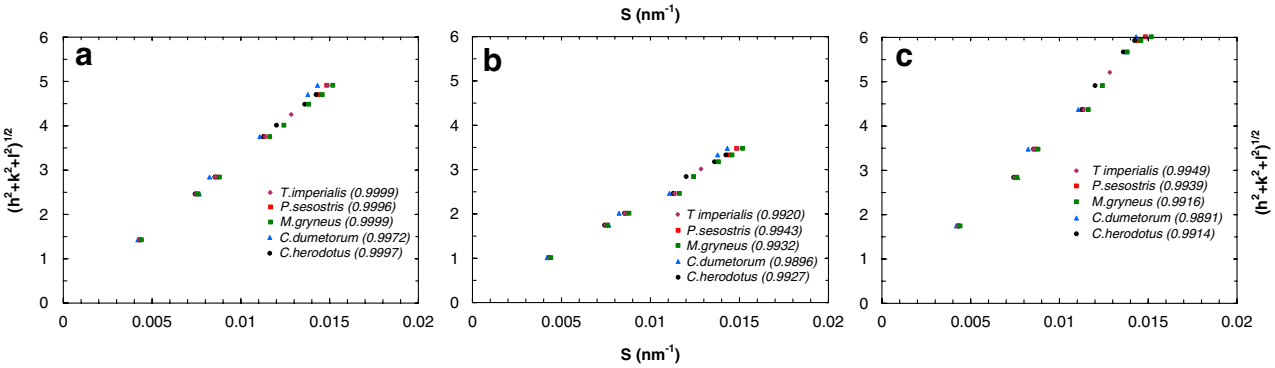

Fig. S4. Indexing of the SAXS azimuthally averaged profiles using the plot of the moduli of the *hkl* Miller indices of the Bragg peak and the corresponding reciprocal lattice spacing, *S*. (*A*) The peaks in the scattering profiles of *Teinopalpus imperialis*, *Parides sesostris, Callophrys (Mitoura) gryneus, Callophrys dumetorum*, and *Cyanophrys herodotus* are shown indexed as the (110), (211), (220), (321), (400), (420), (332), and (422) reflections of the single gyroid ($I4_132$) crystallographic space group symmetry (IUCr International Tables for Crystallography, ref. 2). *B* and *C*, respectively, show the goodness of fit upon reindexing the peaks in the azimuthally averaged profiles as simple primitive (*Pm3m*), and single diamond (*Fd3m*) cubic space groups. The linearity and zero intercepts of the plot confirm the cubic aspect of the nanostructures, but do not specifically discriminate among the possible cubic space groups. However, the slope of this plot gives an estimate of the unit cell lattice parameter (i.e., the length of a side of the cubic unit cell) for the nanostructure, which can be compared to estimates from EM images. The EM-estimated lattice parameters correspond much more closely to the SAXS-estimates of the butterfly nanostructures, assuming a single gyroid space group than simple primitive (*Pm3m*, too small), or single diamond (*Fd3m*, too large) symmetry (Table S2). Furthermore, a *Pm3m* assignment cannot explain the conspicuous absence of the $\sqrt{2}$ reflection and the presence of the forbidden $\sqrt{7}$ peak (Fig. S3; ref. 2), whereas the incongruence of the observed peaks with the predicted $\sqrt{8}$ and $\sqrt{11}$ peaks, and the complete absence of features at the predicted $\sqrt{16}$ and $\sqrt{19}$ peak positions, do not support the assignment of the *Fd3m* space group (Fig. S3; ref. 2).

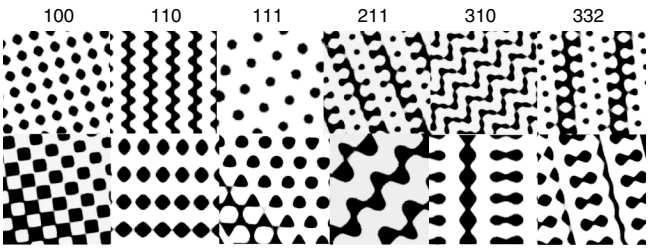

Fig. S5. Simulated (100), (110), (111), (211), (310), and (332) TEM plane projections from level set single diamond (*Fd3m*; *Top*) and simple primitive (*Pm3m*; *Bottom*) cubic space group models with 29% filling fraction for comparison with the butterfly transmission electron micrographs (Fig. 1 *B* and *E*, andFig. S1 *B*, *E*, and *H*). Neither these nor sections through various other crystallographic planes of the *Fd3m* and *Pm3m* geometries could reproduce the complex motifs seen in the butterfly TEM images, unlike sections through the level set single gyroid model (8).

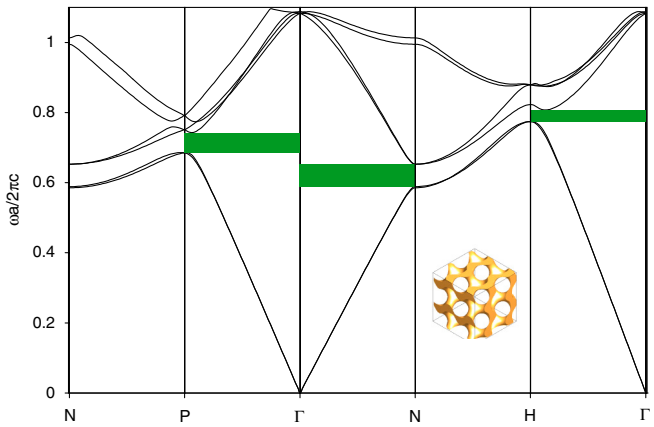

Fig. S6. A representative photonic bandgap diagram for a simulated single gyroid ($I4_132$) nanostructure with a 25% dielectric ($n = 1.56$) filling fraction. The presence of three relatively closely spaced pseudogaps along the Γ-N (110), Γ-P (111), and Γ-H (200) directions is highlighted. The gap widths are given by $\Delta\omega/\omega_{\mathrm{mid}}$. (*Inset*) A volume rendering of the simulated single gyroid photonic nanostructure used for bandgap calculations.

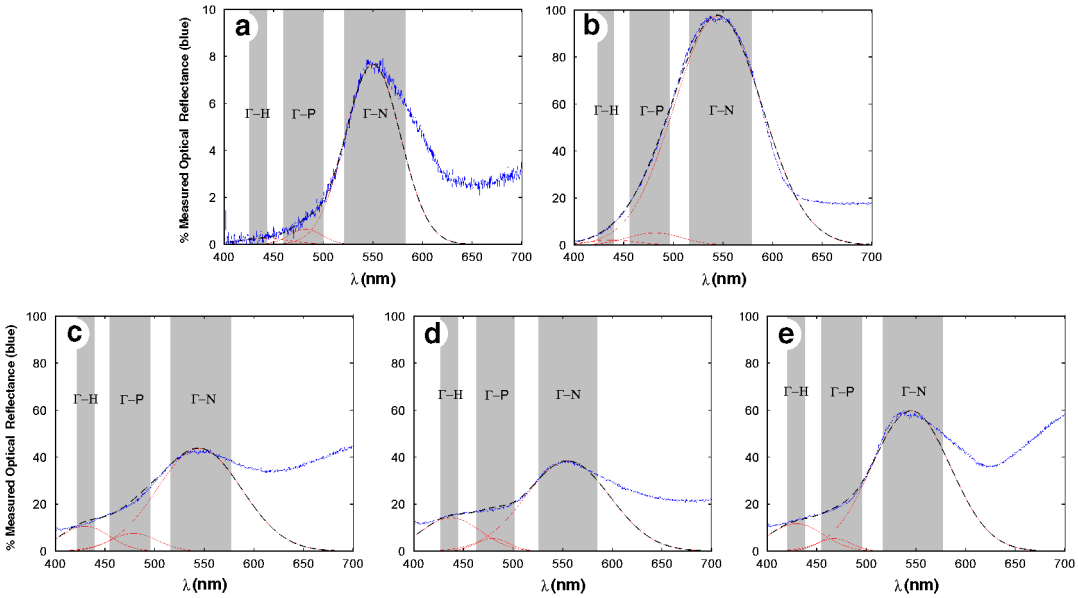

Fig. S7. Measured normal-incidence reflectance spectra (blue line) for (*A*) *Teinopalpus imperialis*, (*B*) *Parides sesostris*, (*C*) *Callophrys (Mitoura) gryneus*, (*D*) *Callophrys dumetorum*, and (*E*) *Cyanophrys herodotus*, with independent Gaussian deconvolutions (red lines) of the reflectance peak and their sums (black dashed lines). The corresponding Γ-N (110), Γ-P (111), and Γ-H (200) bandgaps are highlighted in gray. The independent Gaussian fits to the optical reflectance spectra for all five species coincide fairly well with the three corresponding bandgaps.

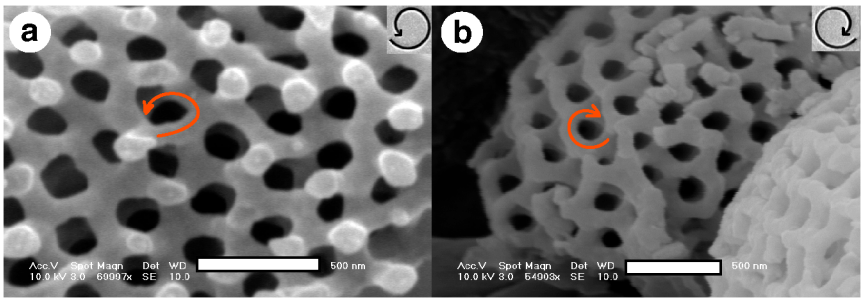

Fig. S8. Chirality of the single gyroid butterfly photonic nanostructures. SEM images of the photonic nanostructures of *C. dumetorum* showing opposite chirality of the single gyroid domains. Chitin channels (gray) in the domains can be seen to spiral or gyrate in a counterclockwise (*A*) or clockwise (*B*) fashion, away from the viewer.

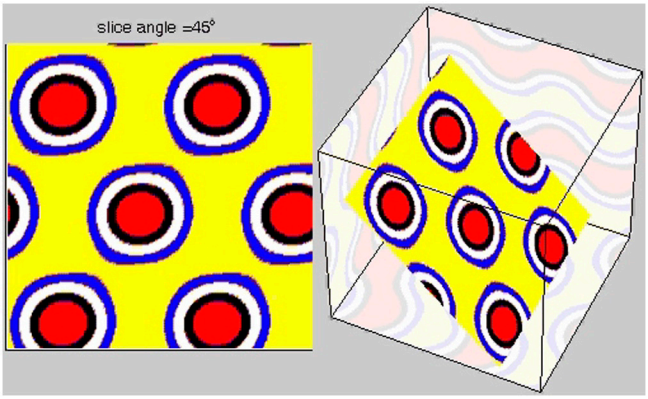

Movie S1. A slice-by-slice movie through the pentacontinuous volume of a level set core-shell double gyroid structure with a 25% core filling fraction ($2 \times 2 \times 2$ unit cells), at slice angles of 45, 30, and 0° to the *x* axis. Each slice is a section through a particular plane of a polarized (ABCB′A′) pentacontinuous core-shell double gyroid model, in which A (red) is the extracellular space, B (black) is the plasma membrane, C (white) is the cytoplasmic intracellular space, B′ (blue) is the smooth endoplasmic reticulum (SER) membrane, and A′ (yellow) is the intra-SER space. Note, the slice angles of 45, 30, and 0° depict the (110), (210), and (100) planes, respectively.

Movie S1 (AVI)

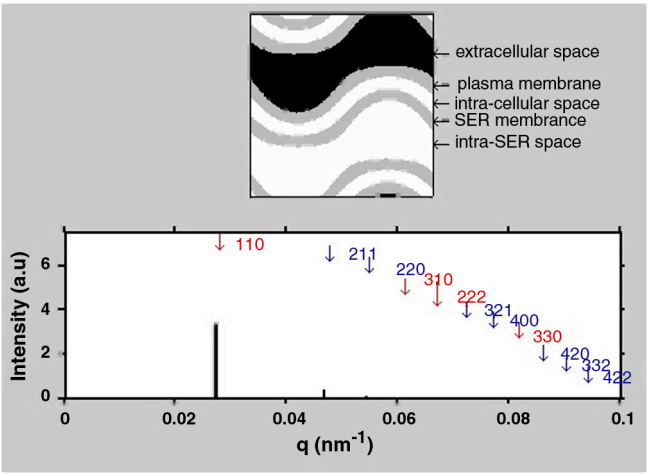

Movie S2. Visualization of the hypothesized transformation of a core-shell double gyroid (*Ia3d*) into a single network gyroid ($I4_132$) structure during the development of butterfly wing scale photonic nanostructure (*Top*, (100) projection) and the corresponding SAXS structure factors during the transition (*Bottom*). The grayscale contrast of the visualized slice represents illustrative electron densities of the butterfly nanostructure as it transitions. In this evolution from a core-shell double gyroid to a single gyroid symmetry, as indicated by the arrows in the simulated SAXS structure factors, initially, the $\sqrt{2}$ (110) peak is noticeably absent, whereas the first two peaks are in the ratios of $\sqrt{6}$ (211) and $\sqrt{8}$ (220), as expected for the double gyroid (*Ia3d*) structure. However, the diagnostic $\sqrt{2}$ (110) peak appears as the first-order peak and gradually grows in intensity during the transition to the single gyroid ($I4_132$) network (2, 9, 10). All of the marked peaks are allowed for the single gyroid space group, whereas the ones marked in red are not permitted for the double gyroid symmetry. The level set gyroid nanostructure model used for this simulation has a core volume fraction of 30% and a lattice parameter of 329 nm. Note that due to the finite resolution of the simulation, many of the higher-order peaks are difficult to discern. The movie continues with a version, where the intensities are log transformed, in order to better discriminate the predicted peaks.

Movie S2 (MOV)

Table S1. Summary of the structural and optical properties of the photonic nanostructure on the wing scales of the five papilionid and lycaenid butterflies assayed in this study

Taxon	Locality	Scale color	λ_{pk}, optical reflectance peak, nm	*a*, lattice parameter*, nm	Bragg diffraction length in units of *a*†, % Γ-N gap width	*D*, Crystallite domain size‡ (μm)	n_{avg} (chitin filling fraction)§
Family papilionidae (Swallowtail butterflies)							
Subfamily Papilioninae							
Teinopalpus imperialis (Hope 1843)	Unknown	Green dorsal	550	330	4.0 (11)	3.3	1.21 (0.31)
Parides sesostris (Cramer 1779)	Brazil	Green dorsal	545	329	4.0 (11)	4.5	1.20 (0.30)
Family lycaenidae (blues and coppers)							
Subfamily theclinae							
Callophrys dumetorum (Boisduval 1852)	Unknown	Green ventral	555	344	4.4 (10)	2.0	1.16 (0.25)
Callophrys (Mitoura) gryneus (Hübner 1819)	Kansas: Douglas County	Green ventral	545	323	3.9 (11)	4.2	1.22 (0.34)
Cyanophrys herodotus (Fabricius, 1793)	Veracruz, Mexico	Green ventral	545	331	4.1 (11)	3.7	1.19 (0.29)

*From the slope of the plot of the moduli of assigned *hkl* indices of SAXS peaks vs. the respective reciprocal distance (Fig S2).
†Given by $2d/(\pi^{*}\Delta\omega/\omega_{mid})$, where $\Delta\omega/\omega_{mid}$ is the Γ-N (110) gap width from bandgap calculations, and *d* is the (110) Bragg spacing $(a/\sqrt{2})$.
‡From the FWHM of pseudo-Voigt fits to the first-order SAXS peaks, $D \approx 2\pi/\Delta q$.
§Estimated from bandgap calculations by choosing a/λ_{pk} as the Γ-N midgap frequency.

Table S2. Estimates of the lattice parameters and chitin filling fractions of the photonic nanostructures on the wing scales of the five papilionid and lycaenid butterflies assayed in this study

Taxon	Single gyroid ($I4_132$) lattice parameter estimate*, nm	Primitive cubic (*Pm3m*) lattice parameter estimate*, nm	Single diamond (*Fd3m*) lattice parameter estimate*, nm	Measured† lattice parameter ± SD (*N*), nm	Published lattice parameter estimates (source), nm	Estimated (published) chitin filling fraction estimates
Family Papilionidae						
Teinopalpus imperialis	330	230	399	279 ± 22 (12)	268 ± 25 (11)‡	0.31 (0.31)§
Parides sesostris	329	229	401	288 ± 48 (16)	260 ± 63 (5)	0.3 (0.4)§
Family Lycaenidae						
Callophrys dumetorum	344	237	414	291 ± 9 (5)	363 ± 45 (5)¶	0.25 (0.17)§,¶
Callophrys (Mitoura) gryneus	323	226	397	306 ± 33 (10)	363 ± 45 (5)¶	0.34 (0.17)§,¶
Cyanophrys herodotus	331	231	407	298 ± 41 (5)	395 (7)	0.29 (not available)

*From indexing the SAXS data, see Fig. S4.
†From an analysis of our scanning electron micrographs of the butterflies, *N* is the sample size.
‡Average dimensions of the diagnosed triclinic lattice unit cell (see ref. 11).
§Values from ref. 5.
¶Values for *Callophrus rubi*, a close congener of *C. dumetorum* and *C. gryneus*.